RSC Advances

PAPER

View Article Online
View Journal | View Issue

Cite this: *RSC Adv.*, 2016, **6**, 106364

One-step synthesis and the enhanced xylene-sensing properties of Fe-doped MoO_3 nanobelts

Ruiliang Xu,[a] Nan Zhang,[a] Liang Sun,[c] Chuan Chen,[c] Yu Chen,*[ac] Chuannan Li*[a] and Shengping Ruan*[ab]

Received 6th September 2016
Accepted 27th October 2016

DOI: 10.1039/c6ra22268d

www.rsc.org/advances

Pure and Fe-doped MoO_3 nanobelts were synthesized by a facile one-step hydrothermal method and their xylene-sensing properties were investigated. Different Fe-doping contents were introduced into MoO_3 nanobelts to study their effect on morphology and xylene sensitivity. With an increase in Fe-doping content, the width of the MoO_3 nanobelts became larger and excess Fe-doping even made the nanobelts start to turn into nanosheets. For xylene detection, Fe-doping content also had an effect on the performance of MoO_3 nanobelts and a proper Fe-doping content could effectively enhance their sensitivity to xylene, such as higher response and better selectivity than the pure MoO_3 nanobelts. In addition, the enhanced xylene-sensing properties induced by Fe-doping are also discussed.

Introduction

With the advance in society, the relation between environmental pollution and human health has become a more and more important topic. Air pollution induced by the emissions of toxic inorganic gases (like NO_x, SO_2 and CO) and volatile organic compounds (VOCs) (like acetone, benzene and xylene) is an intractable problem.[1–4] As a momentous material, xylene is closely related to our daily lives. It is extensively used in pigments, oil paints, the rubber industry and aircraft fuel, but it is also highly toxic.[5] A certain concentration of xylene can cause serious diseases like pneumonia and cancer, and even a little xylene can lead to vomiting and neurasthenia.[5] The damage that xylene can do to the human body is easy to find, whether to the workers in chemical plants or to ordinary people in everyday life. Therefore, it is significant to detect and monitor xylene.

There are many known methods in xylene detection, such as double layered metal-oxide thin film technology,[6] solid-state chemical technology,[7] and micro-fabricated preconcentrator technology.[8] It is worth noting that these methods are dangerous to the users and inconvenient to operate. Gas sensors based on metal oxide semiconductors, such as SnO_2, TiO_2, ZnO, In_2O_3, WO_3,[9–13] show their superiority in terms of low cost, easy fabrication, environmental friendliness and high performance, making them a promising way to detect poisonous and flammable gases. In recent years, due to the enhanced or emerging properties induced by their small size and large surface-to-volume ratio, metal oxide semiconductor nanomaterials, especially those with one-dimensional (1-D) nanostructures (including nanowires, nanofibers, nanotubes and nanobelts), have attracted people's interest in their research and application in the chemical, mechanical, optical, electrical and sensing fields.[14,15]

Molybdenum trioxide (MoO_3) is one of the most intriguing transition-metal oxides with important properties like catalysis, electrochromism, photochromism and thermochromism, and has found uses in various fields such as catalysis,[16] gas sensing,[17] field emission,[18] lithium-ion batteries,[19] photochromic devices,[20] and electrochromic devices.[21] There are three main polymorphs of MoO_3: orthorhombic α-MoO_3 (the thermodynamically stable phase), monoclinic β-MoO_3, and hexagonal h-MoO_3 (low temperature metastable phases).[22,23] With a wide band gap of 2.8–3.6 eV, α-MoO_3 is widely used as an n-type metal oxide semiconductor in detecting varieties of gas such as H_2,[24] H_2S,[25–27] NO_2,[28] ethanol,[29] and TMA.[30] However, the pure metal oxide semiconductor based sensor is usually unsatisfactory because of its low response, poor selectivity, slow response and recovery rate and so on. So, researchers have been making great efforts to improve the gas sensing properties of metal oxide semiconductors.

Doping has been proved to be a simple and effective way to improve the electrical, catalytic and optical performance of base materials.[31–34] As an inexpensive and effective dopant, iron (Fe) has been used in the gas sensing field to improve the sensitivity performance of base materials such as ZnO,[35] WO_3,[36] and SnO_2.[37] For example, it has been reported that a gas sensor based on Fe-doped SnO_2 nanostructures exhibited highly selective sensing behavior towards hydrogen sulfide (H_2S).[38]

In this study, pure and Fe-doped α-MoO_3 nanobelts with different Fe-doping contents were successfully synthesized. And

[a]State Key Laboratory on Integrated Optoelectronics, College of Electronic Science & Engineering, Jilin University, Changchun 130012, P. R. China. E-mail: ruansp@jlu.edu.cn; licn@jlu.edu.cn; chenyu@semi.ac.cn
[b]State Key Laboratory on Applied Optics, Changchun 130023, P. R. China
[c]Global Energy Interconnection Research Institute, Beijing, 102211, P. R. China

the effects of Fe-doping content on the microscopic morphology and xylene-sensing properties were investigated in detail. The result revealed that the MoO_3 nanobelts with a proper Fe-doped content showed a higher response and better selectivity to xylene than the pure MoO_3 nanobelts. In addition, the sensitive mechanism of MoO_3 and Fe-doped MoO_3 to xylene is discussed.

Experimental section

Synthesis of pure and Fe-doped α-MoO_3 nanobelts

The pure and Fe-doped α-MoO_3 nanobelts were both synthesized by a simple one-step hydrothermal method. Firstly, 0.618 g of ammonium molybdate tetrahydrate ($(NH_4)_6Mo_7O_{24}\cdot 4H_2O$) were dissolved into 25 mL of deionized water under stirring for about 30 minutes to achieve an aqueous solution. In the Fe-doped α-MoO_3 nanobelts case, a certain amount of ferric nitrate nonahydrate ($Fe(NO_3)_3\cdot 9H_2O$) needed to be dissolved into the solution. Secondly, 2.5 mL of nitric acid (HNO_3) were added into the above solution dropwise under stirring to adjust the PH. Then, the solution was transferred into a 50 mL of Teflon-lined stainless steel autoclave and disposed by hydrothermal treatment for 36 h at 180 °C.

When the autoclave cooled down to room temperature, the precipitates were centrifuged and washed with deionized water 5 times and then the precipitates were dried at 80 °C for 12 h. Finally, the products were annealed at 300 °C for 2 h at a heating rate of 1 °C min^{-1} to obtain the pure or Fe-doped α-MoO_3 nanobelts.

To investigate the effects of Fe-doping content on the crystal structure, the morphology and xylene-sensing properties of the MoO_3 nanobelts, 1, 3, 5, 10 and 15 wt% (weight ratio to $(NH_4)_6Mo_7O_{24}\cdot 4H_2O$) of $Fe(NO_3)_3\cdot 9H_2O$ were respectively added in the synthetic process to obtain MoO_3 nanobelts with different Fe-doping content, and the corresponding samples were denoted as 1Fe–MoO_3 NBs, 3Fe–MoO_3 NBs, 5Fe–MoO_3 NBs, 10Fe–MoO_3 NBs and 15Fe–MoO_3 NBs.

Characterization

X-ray diffraction was used to identify the phase of the samples (Scintag XDS-2000 X-ray diffractometer with Cu Kα1 radiation (λ = 1.5406 Å). Scanning electron microscopy was used to investigate the morphologies of the samples (JEOL JSM-7500F microscope operating at 15 kV).

Fabrication and measurement of gas sensors

First, deionized water and ready-made material were mixed at a weight ratio of 4 : 1 and then ground in a mortar for about 5 minutes to form a paste. After that, the paste was coated onto the surface of a ceramic tube with a pair of parallel golden electrodes. Finally, an Ni–Cr alloy heating coil was inserted through the ceramic tube, and was welded onto a pedestal together with the ceramic tube. The structure of the sensor device is shown in Fig. 1.

The gas sensing performance testing of the samples was conducted on a CGS-8 Intelligent Gas Sensing Analysis System (Beijing Elite Tech Co., Ltd., China). The system can control the operating temperature of the sensor by adjusting the current of the heating coil and collecting the real-time resistance of the sensor. The response of the sensor was expressed as the value of R_a/R_g (R_a represents the resistance of the sensor in air and R_g represents the resistance of the sensor in the test gas). The response time was defined as the time for the resistance value to increase from 10% to 90% of the total change ($R_a - R_g$), when the sensors were exposed to the test gas. And the recovery time was defined as the time for the resistance value to decrease from 90% to 10% of the total change, when the sensor was exposed to air again.

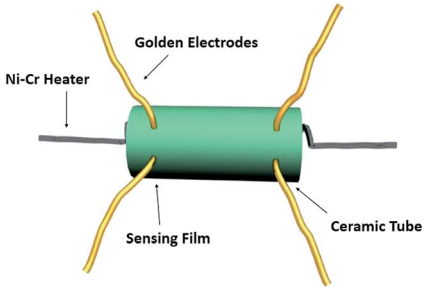

Fig. 1 Structure of a heater-type gas sensor after coating with the sensing film.

Results and discussion

Materials characterizations

Fig. 2(a) shows the morphology of the pure α-MoO_3 nanobelts, and Fig. 2(b)–(f) show the morphologies of the Fe-doped α-MoO_3 nanobelts with an increasing Fe-doping content. Fig. 2(a) reveals that the as-synthesized pure MoO_3 showed a belt-like morphology whose average width and length were about 350 nm and 8 μm, respectively. For the Fe-doped α-MoO_3 with a lower Fe-doping content (5 wt% or less), as shown in Fig. 2(b)–(d), the morphology of the samples was also nanobelt. And it is worth noting that the breadth of the samples gradually increased with the increase in Fe-doping content. For the Fe-doped α-MoO_3 with a higher Fe-doping content (10 wt% or more) shown in Fig. 2(e) and (f), the breadth of the samples further increased with the increase in Fe-doping content, which

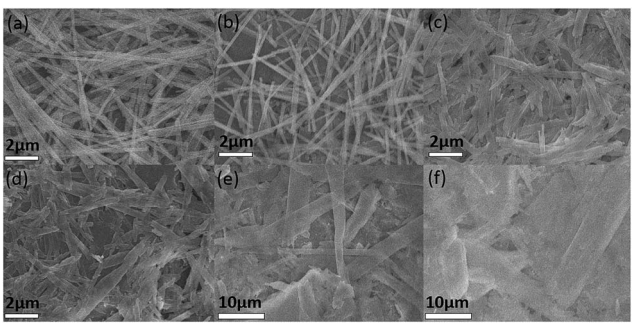

Fig. 2 SEM images of (a) pure α-MoO_3 nanobelts and (b)–(f) Fe doped α-MoO_3 nanobelts, respectively.

made the samples tend to turn into a sheet-like morphology with aggravated aggregation. Such a result reveals that Fe-doping could obviously influence the morphology.

Fig. 3 shows the XRD patterns of both pure and Fe-doped MoO_3 nanobelts. It can be seen that all of the diffraction peaks of each product were consistent with the standard diffraction peaks of α-MoO_3 from the Joint Committee on Powder Diffraction Standards card (JCPDS, no. 05-0503). For the Fe-doped MoO_3 nanobelts, significant Fe-based oxides, such as Fe_2O_3 and Fe_3O_4 peaks, were not found. It is worth noting that, compared with the pure MoO_3, the relative intensity of the (0 2 0), (0 4 0), (0 6 0) and (1 10 0) peaks gradually decreases with the increase in Fe-doping amount, indicating reduced crystallinity and orientation.

Further microscopic morphological and structural characterization of 5Fe–MoO_3 NBs was carried out by TEM and high-resolution TEM (HRTEM), as shown in Fig. 4(a) and (b), respectively. The distinct lattice stripes in the HRTEM image imply high crystallinity. The measured interplanar distance of 0.198 nm and 0.183 nm in the selected region was in good agreement with the theoretical d spacing of the (001) and (100) lattice planes of an orthorhombic MoO_3 crystal.

In order to test the valence state of Fe, Mo and O in MoO_3 nanobelts, we measured the XPS of the samples. Fig. 5(a), (b) and (c) shows the XPS analysis of Mo 3d peaks, O 1s peak and Fe 2p for MoO_3 nanobelts annealed at 300 °C, respectively. As shown in Fig. 5(a), no peak corresponding to Mo metal has been formed. And two patterns of Mo 3d are observed, which are attributed to two components of Mo $3d_{5/2}$ and $3d_{3/2}$. Solid lines (the dominant peaks) at 232.8 ± 0.1 and 236.1 ± 0.1 eV represent the major component corresponding to Mo^{6+} ions. While dashed lines (recessive peaks) shift to lower binding energies and are attributed to Mo^{5+} ions. Fig. 5(b) presents XPS spectra in the O 1s energy, and peaks associated with oxides and chemisorbed oxygen can be distinguished. The peaks shown by solid lines at 531.2 ± 0.1 eV are assigned to lattice oxygen atoms of MoO_3. The corresponding XPS spectra in the Fe 2p energy region are shown in Fig. 5(c). The peaks shown by solid lines at 713.8 ± 0.1 eV are assigned to Fe^{2+} ions. In addition, according to the XPS characterization, the atom ratios of Fe to Mo were about 2.67%, 2.93%, 3.14%, 3.61% and 4.22% for the samples with increasing Fe-doping content.

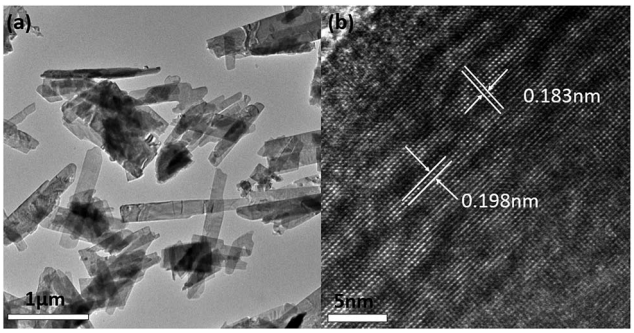

Fig. 4 (a) TEM and (b) HRTEM images of 5Fe–MoO_3 NBs.

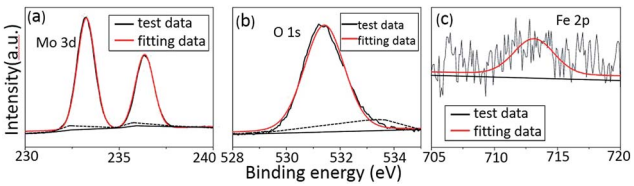

Fig. 5 XPS spectra of the element Mo, O and Fe.

Gas sensing properties

Operating temperature has a significant influence on gas sensing properties (such as response value, response and recovery rate and selectivity) of semiconductor materials, so it is of primary importance to determine the optimal operating temperature of a sensor.

Fig. 6 shows the response value of pure and Fe-doped α-MoO_3 nanobelts in different operating temperatures. As can be seen, the responses increase as the operating temperature increases from 136 °C to 206 °C for both sensors. However, when the temperature is higher than 206 °C, the responses mightily decrease along with the increasing temperature. The reason for response increase first and then decrease is that, when the temperature was rising, the speed of molecular

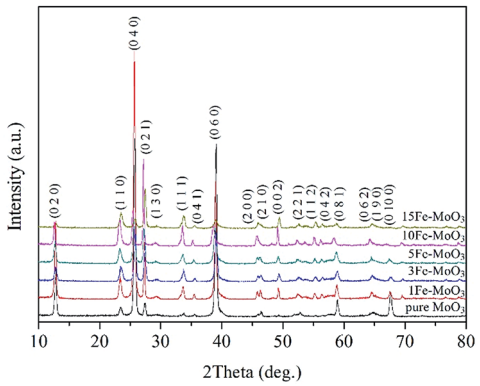

Fig. 3 XRD patterns for both pure α-MoO_3 nanobelts and Fe-doped α-MoO_3 nanobelts.

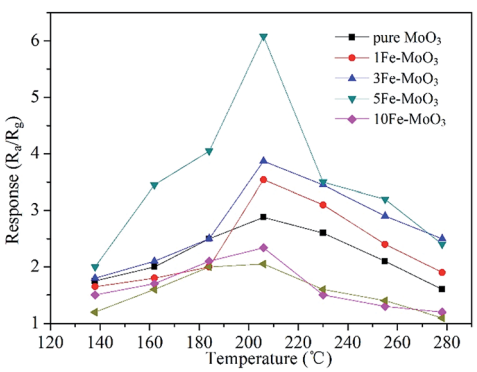

Fig. 6 Response of both pure α-MoO_3 nanobelts and Fe-doped α-MoO_3 nanobelts in 100 ppm xylene at different temperatures.

vibration would increase at the same time which would improve the chemical reaction between the sensor and test gas. Hence, active reaction would lead to the response increasing. However, when the temperature continued to go up, the reaction was so fast that the penetration was less related to the entire sensing film. Therefore, with the subdued reaction, the response became lower.

As a result, we can draw a conclusion that the best operating temperature for both sensors is 206 °C. Among all the sensors, the one based on 5Fe–MoO_3 NBs showed the highest response to 100 ppm xylene. The maximum response values of pure MoO_3 NBs and 5Fe–MoO_3 NBs were 2.9 and 6.1, respectively, which means that the response of Fe-doped α-MoO_3 nanobelts was twice as high as that of pure α-MoO_3 NBs. In addition, it is worth noting that, excess Fe-doping content could lead to a decrease in response.

Fig. 7 shows the responses of pure and Fe-doped α-MoO_3 NBs when they were tested in different concentrations of xylene at 206 °C. The response values for both sensors increased rapidly as the concentrations of xylene changed from 5 ppm to 200 ppm and then tended to saturation as the concentrations of xylene went over 500 ppm. In addition, at each xylene concentration, 5Fe–MoO_3 NBs gave the highest response among the sensors.

In practical application, selectivity is very important because it reflects the ability of a sensor to identify the target gas. Good selectivity means that the gas sensor can provide precise information about the ambience and it will benefit the following process (such as sending an alert). The responses of pure and Fe-doped α-MoO_3 NBs based sensors to 100 ppm different interference gases, including formaldehyde (HCHO), acetylene (C_2H_2), carbon monoxide (CO), nitrogen dioxide (NO_2), methane (CH_4), ammonia (NH_3) and sulfur dioxide (SO_2), are shown in Fig. 8. It can be seen that the 5Fe–MoO_3 NBs based sensor, whose response to xylene (reaching 6.1) was several times as high as the responses to other gases (less than 2), showed much better selectivity than the other sensors.

The response time and recovery time of a gas sensor are of great significance for real-time detection and in particular a short response time means that the sensor can provide a timely alert. The response and recovery properties of pure and

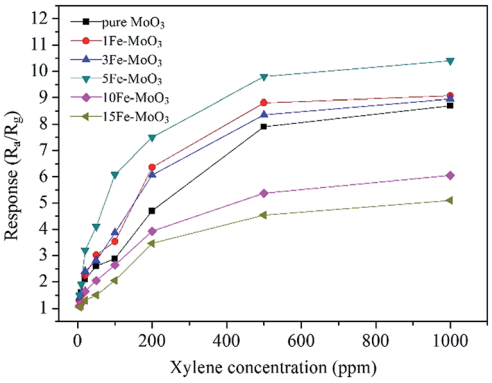

Fig. 7 Response of pure α-MoO_3 nanobelts and Fe-doped α-MoO_3 nanobelts at 206 °C in different concentration of xylene.

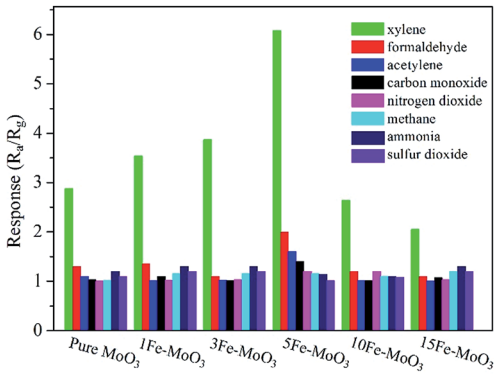

Fig. 8 Response of sensors based on Fe-doped α-MoO_3 nanobelts at 206 °C towards various test gases.

Fe-doped MoO_3 NBs against 20, 50 and 100 ppm are shown in Fig. 9. This indicates that the responses of the sensors increased rapidly when the sensor was shifted from air to xylene ambience and the responses gradually decreased when the sensor was exposed to the air again. The data showed that both the response and the recovery times of Fe-doped MoO_3 are longer than those of the pure MoO_3. The typical response and recovery times of 5Fe–MoO_3 NBs to 100 ppm xylene were 20 s and 75 s, while response and recovery times of pure MoO_3 nanobelts were 6 s and 40 s, respectively. In addition, a comparison of some reported xylene sensors with the Fe-doped MoO_3 nanobelts is shown in Table 1.

An applied sensor has to face a complex working environment and the effect of humidity on gas sensing properties is unavoidable. Fig. 10 shows the response of pure and Fe-doped MoO_3 NBs based sensors when they worked in different humidities. The results showed the as-fabricated sensors could work well in a low humidity environment, and the response gradually decreased with the rise in relative humidity.

Gas sensing mechanism

The gas sensing mechanism of pure and Fe-doped MoO_3 nanobelts can be explained through a surface-controlled mode,

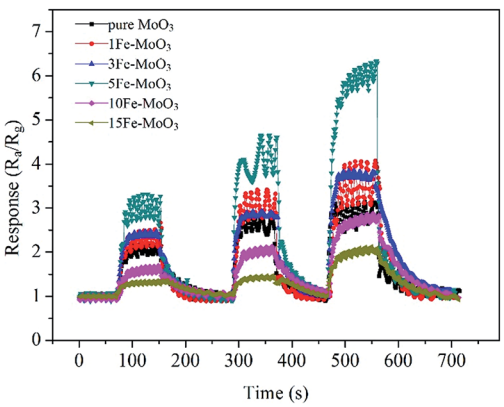

Fig. 9 Transient response curves of the pure and Fe-doped α-MoO_3 nanobelt sensors when they were tested in 20, 50 and 100 ppm xylene at 206 °C.

Table 1 A comparison between the as-fabricated Fe-doped MoO_3 nanobelts based sensors and reported xylene sensors in the literature

Materials	Synthetic method	Working temperature	Response to 100 ppm xylene	Response/recovery time
Co_3O_4 nanocubes[39]	Microwave-assisted solvothermal method	200 °C	6.45	—
SnO_2 nanoparticles/MWCNT[40]	—	220 °C	3.4	25 s/100 s
ZnO nanorods[41]	Solid-state chemical reaction method	150 °C	9.6	7 s/20 s
Ni-doped TiO_2 microbowls[42]	Electrospray	302 °C	4.4	9 s/1.2 s
This work Pure MoO_3 NBs	Hydrothermal method	206 °C	2.9	6 s/40 s
1Fe–MoO_3 NBs			3.54	14 s/42 s
3Fe–MoO_3 NBs			3.87	17 s/90 s
5Fe–MoO_3 NBs			6.1	20 s/75 s
10Fe–MoO_3 NBs			2.64	22 s/96 s
15Fe–MoO_3 NBs			2.05	27 s/90 s

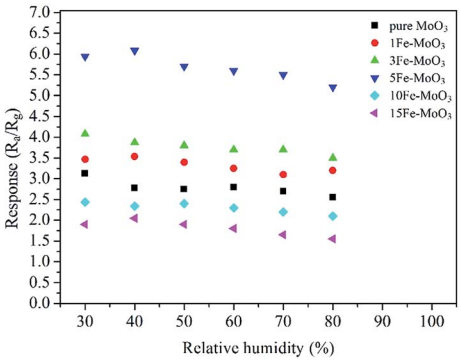

Fig. 10 Response of sensors based on Fe-doped α-MoO_3 nanobelts working in different humidity.

which involves gas adsorption, electronic transfer and gas desorption *etc.*[43,44]

MoO_3 is a kind of n-type semiconductor and its conductivity or resistance is mainly dependent on the electron which is the majority carrier. When the sensors are exposed to air, oxygen molecules (O_2) will adsorb onto the surface and then ionize into O_2^-, O^- or O^{2-} (depending on the temperature[45]) by capturing free electrons from the conduction band of MoO_3. The reaction equations are as follows:

$$O_2\ (gas) \rightarrow O_2\ (ads) \quad (1)$$

$$O_2\ (ads) + e^- \rightarrow O_2^-\ (ads),\ (T < 100\ ^\circ C) \quad (2)$$

$$O_2^-\ (ads) + e^- \rightarrow 2O^-\ (ads),\ (100\ ^\circ C < T < 300\ ^\circ C) \quad (3)$$

$$O^-\ (ads) + e^- \rightarrow O^{2-}\ (ads),\ (T > 300\ ^\circ C) \quad (4)$$

As the same time, due to the decrease in electronic concentration, an electronic depletion layer will form at the surface of the MoO_3 nanobelts. As a result, the resistances of both pure and Fe-doped α-MoO_3 nanobelts sensors show high values.

When the sensors are operating at 206 °C and transferred into a xylene ambience, xylene molecules will react with the ionized oxygen species (O^- is dominant). That will lead to the electrons captured by the ionized oxygen species being released back to the pure and Fe-doped MoO_3 nanobelts. And as a result, the width of the electronic depletion layer shrinks and the resistance decreases. The corresponding reaction is as follows:[41]

$$C_8H_{10} + 21O^- \rightarrow 8CO_2 + 5H_2O + 21e^- \quad (5)$$

When the sensors are out of the xylene ambience and exposed to air, oxygen-ions will form on the surface of the nanobelts again and the sensor's resistance recovers to the initial value.

The possible reason for the enhanced response of MoO_3 nanobelts induced by Fe-doping can be explained as follows: because the valance of Fe^{2+} is lower than Mo^{5+} and Mo^{6+}, when Fe^{2+} enters into the lattice of MoO_3 and replaces Mo^{5+} or Mo^{6+}, it will act as a dopant providing holes. As a result, the concentration of the major carrier electrons of the n-type MoO_3 decreases and makes the Fe-doped MoO_3 nanobelts show high resistance. So, when the Fe-doped MoO_3 nanobelts come into contact with the reduced xylene molecules, a greater change in resistance or a higher response will be obtained compared with the pure MoO_3 nanobelts. In addition, the smaller ionic radius of Fe^{2+} will induce lattice distortion, which will influence the electric and absorption properties of the MoO_3 and make it more active.

In addition, according to the research reported by Yang *etc.*,[46] Mo^{5+} in α-MoO_3 lattice is the favourite absorption site for oxygen species and it will lead to more chemisorbed oxygen on the surface of the nanobelts and thus improves the xylene response. Also, the higher specific surface area of the nanobelts contributes to the enhanced response by providing more absorption sites.

Conclusions

In conclusion, the pure MoO_3 nanobelts and Fe-doped MoO_3 nanobelts with different Fe-doping content were successfully synthesized by a one-step hydrothermal process and their xylene-sensing properties were investigated in detail. The results showed that the Fe-doping had great effects on morphology, crystallinity and xylene sensitivity. For xylene

detection, MoO_3 with a proper Fe-doping content, especially the 5Fe–MoO_3 NBs, showed a double response and better selectivity to xylene at 206 °C, which made the Fe-doped α-MoO_3 nanobelts based sensor a better candidate for xylene detection.

Acknowledgements

This work was supported by the National Natural Science Foundation of China (Grant No. 11574110), Project of Science and Technology Development Plan of Jilin Province (Grant No. 20160204013GX), Project of Statistic Analysis of Gas Sensitive Materials, Opened Fund of the State Key Laboratory on Applied Optics and Opened Fund of the State Key Laboratory on Integrated Optoelectronics (No. IOSKL2013KF10).

Notes and references

1 J. Schalwig, S. Ahlers, P. Kreisl, C. B.-v. Braunmühl and G. Müller, *Sens. Actuators, B*, 2004, **101**, 63.
2 N. Rezlescu, N. Iftimie, E. Rezlescu, C. Doroftei and P. D. Popa, *Sens. Actuators, B*, 2006, **114**, 427.
3 M. T. Ke, M. T. Lee, C. Y. Lee and L. M. Fu, *Sensors*, 2009, **9**, 2895.
4 Y. Cao, P. Hu, W. Pan, Y. Huang and D. Jia, *Sens. Actuators, B*, 2008, **134**, 462.
5 M. Gérin, J. Siemiatycki, M. Désy and D. Krewski, *Am. J. Ind. Med.*, 1998, **34**, 144.
6 T. Akiyama, Y. Ishikawa and K. Hara, *Sens. Actuators, B*, 2013, **181**, 348.
7 J. Hue, M. Dupoy, T. Bordy, R. Rousier, S. Vignoud, B. Schaerer, T. H. Tran-Thi, C. Rivron, L. Mugherli and P. Karpe, *Sens. Actuators, B*, 2013, **189**, 194.
8 C. E. Davis, C. K. Ho, R. C. Hughes and M. L. Thomas, *Sens. Actuators, B*, 2005, **104**, 207.
9 C. S. Rout, A. Govindaraj and C. N. R. Rao, *J. Mater. Chem.*, 2006, **16**, 3936.
10 C. S. Rout, M. Hegde and C. N. R. Rao, *Sens. Actuators, B*, 2008, **128**, 488.
11 C. S. Rout, M. Hegde, A. Govindaraj and C. N. R. Rao, *Nanotechnology*, 2007, **18**, 205504.
12 C. S. Rout, G. U. Kulkarni and C. N. R. Rao, *J. Phys. D: Appl. Phys.*, 2007, **40**, 2777.
13 C. S. Rout, K. Ganesh, A. Govindaraj and C. N. R. Rao, *Appl. Phys. A: Mater. Sci. Process.*, 2006, **85**, 241.
14 M. W. Ahn, K. S. Park, J. H. Heo, J. G. Park, D. W. Kim, K. J. Choi, J. H. Lee and S. H. Hong, *Appl. Phys. Lett.*, 2008, **93**, 263103.
15 B.-Y. Wei, M.-C. Hsu, P.-G. Su, H.-M. Lin, R.-J. Wu and H.-J. Lai, *Sens. Actuators, B*, 2004, **101**, 81.
16 G. Jin, G. Lu, Y. Guo, J. Wang and X. Liu, *Catal. Lett.*, 2003, **87**, 249.
17 E. Comini, L. Yubao, Y. Brando and G. Sberveglieri, *Chem. Phys. Lett.*, 2005, **407**, 368.
18 Y. B. Li, Y. Bando, D. Golberg and K. Kurashima, *Appl. Phys. Lett.*, 2002, **81**, 5048.
19 D. Mariotti, H. Lindstrom, A. C. Bose and K. K. Ostrikov, *Nanotechnology*, 2008, **19**, 495302.
20 L. Zheng, Y. Xu, D. Jin and Y. Xie, *Chem. Mater.*, 2009, **21**, 5681.
21 T. Ivanova, K. A. Gesheva, G. Popkirov, M. Ganchev and E. Tzvetkova, *Mater. Sci. Eng., B*, 2005, **119**, 232.
22 P. Badica, *Cryst. Growth Des.*, 2007, **7**, 794–801.
23 X. W. Lou and H. C. Zeng, *Chem. Mater.*, 2002, **14**, 4781.
24 M. B. Rahmani, S. H. Keshmiri, J. Yu, A. Z. Sadek, L. Al-Mashat, A. Moafi, K. Latham, Y. X. Li, W. Wlodarski and K. Kalantar-zadeh, *Sens. Actuators, B*, 2010, **145**, 13.
25 W.-S. Kim, H.-C. Kim and S.-H. Hong, *J. Nanopart. Res.*, 2009, **12**, 1889.
26 M. MalekAlaie, M. Jahangiri, A. M. Rashidi, A. HaghighiAsl and N. Izadi, *Mater. Sci. Semicond. Process.*, 2015, **38**, 93.
27 S. Bai, C. Chen, R. Luo, A. Chen and D. Li, *Sens. Actuators, B*, 2015, **216**, 113.
28 S. Bai, S. Chen, L. Chen, K. Zhang, R. Luo, D. Li and C. C. Liu, *Sens. Actuators, B*, 2012, **174**, 51.
29 A. D. Rushi, K. P. Datta, P. S. Ghosh, A. Mulchandani and M. D. Shirsat, *J. Phys. Chem. C*, 2014, **118**, 24034.
30 Y. H. Cho, Y. N. Ko, Y. C. Kang, I.-D. Kim and J.-H. Lee, *Sens. Actuators, B*, 2014, **195**, 189.
31 S. T. Shishiyanu, T. S. Shishiyanu and O. I. Lupan, *Sens. Actuators, B*, 2005, **107**, 379.
32 H. Gong, J. Q. Hu, J. H. Wang, C. H. Ong and F. R. Zhu, *Sens. Actuators, B*, 2006, **115**, 247.
33 A. M. Ruiz, G. Sakai, A. Cornet, K. Shimanoe, J. R. Morante and N. Yamazoe, *Sens. Actuators, B*, 2003, **93**, 509.
34 Q. Wan and T. H. Wang, *Chem. Commun.*, 2005, 3841.
35 P. P. Sahay and R. K. Nath, *Sens. Actuators, B*, 2008, **134**, 654.
36 M. Ahsan, T. Tesfamichael, M. Ionescu, J. Bell and N. Motta, *Sens. Actuators, B*, 2012, **162**, 14.
37 C. Zhao, W. Hu, Z. Zhang, J. Zhou, X. Pan and E. Xie, *Sens. Actuators, B*, 2014, **195**, 486.
38 M. V. Vaishampayan, R. G. Deshmukh, P. Walke and I. S. Mulla, *Mater. Chem. Phys.*, 2008, **109**, 230.
39 C. Sun, X. Su, F. Xiao, C. Niu and J. Wang, *Sens. Actuators, B*, 2011, **157**, 681.
40 K. Y. Choi, J. S. Park, K. B. Park, H. J. Kim, H. D. Park and S. D. Kim, *Sens. Actuators, B*, 2010, **150**, 65.
41 Y. Cao, P. Hu, W. Pan, Y. Huang and D. Jia, *Sens. Actuators, B*, 2008, **134**, 462.
42 L. Zhu, D. Zhang, Y. Wang, C. Feng, J. Zhou, C. Liu and S. Ruan, *RSC Adv.*, 2015, **5**, 28105.
43 J. F. Chang, H. H. Kuo, I. C. Leu and M. H. Hon, *Sens. Actuators, B*, 2002, **84**, 258.
44 J. Zhao, A. Buldum, J. Han and J. P. Lu, *Nanotechnology*, 2002, **13**, 195.
45 Y. Sui, Y. Zeng, L. Fu, W. Zheng, D. Li, B. Liu and B. Zou, *RSC Adv.*, 2013, **3**, 18651.
46 S. Yang, Z. Wang, Y. Hu, X. Luo, J. Lei, D. Zhou, L. Fei, Y. Wang and H. Gu, *ACS Appl. Mater. Interfaces*, 2015, **7**, 9247.